Available online at www.sciencedirect.com
SCIENCE DIRECT®
Journal of Nuclear Materials 340 (2005) 187–202
journal of nuclear materials
www.elsevier.com/locate/jnucmat

Thermal conductivity degradation of ceramic materials due to low temperature, low dose neutron irradiation

L.L. Snead [a,*], S.J. Zinkle [a], D.P. White [b]

[a] Metals and Ceramics Division, Oak Ridge National Laboratory, P.O. Box MS 6087, Oak Ridge, TN 37831-6138, USA
[b] Department of Physics, Merrimack College, North Andover, MA 01845, USA

Received 17 September 2004; accepted 10 November 2004

Abstract

The thermal conductivity degradation due to low-temperature neutron irradiation is studied and quantified in terms of thermal resistance terms. Neutron irradiation is assumed to have no effect on umklapp scattering. A theoretical model is presented to quantify the relative phonon-scattering effectiveness of the three dominant defect types produced by neutron irradiation: point defects, dislocation loops and voids. Several commercial ceramics have been irradiated with fission reactor fast neutrons at low temperatures to produce defects. Materials include silicon carbide, sapphire, polycrystalline alumina, aluminum nitride, silicon nitride, beryllium oxide, and a carbon fiber composite. The neutron dose corresponded to 0.001 and 0.01 displacements per atom (dpa) for a ~60 °C irradiation and 0.01 and 0.1 dpa for a ~300 °C irradiation. Substantial thermal conductivity degradation occurred in all of the materials except BeO following irradiation at 60 °C to a dose of only 0.001 dpa. The data are discussed in terms of the effective increase in thermal resistance caused by the different irradiation conditions. Evidence for significant point defect mobility during irradiation at 60 and 300 °C was obtained for all of the ceramics. The thermal stability of the radiation defects was investigated by isochronal annealing up to 1050 °C.

1. Introduction and theory

Due to the low density of conduction band electrons in most ceramic materials, the dominant carrier of thermal energy is phonons. The lattice thermal conductivity is given by [1,2]:

$$K(T) = \frac{1}{3}\int S(\omega)v^2(\omega)\tau(\omega)\mathrm{d}\omega, \tag{1}$$

where $S(\omega)\mathrm{d}\omega$ is the contribution to the lattice specific heat in the frequency range $\mathrm{d}\omega$ at ω, v is the phonon velocity and $\tau(\omega)$ is the phonon relaxation time. If more than one process is scattering phonons the effective value of $1/\tau(\omega)$ is found by adding $1/\tau_i(\omega)$ for each scattering process, i.e., [1,2]

$$\frac{1}{\tau(\omega)} = \sum_i \frac{1}{\tau_i(\omega)}. \tag{2}$$

The radiation-induced defects to be considered here are, point defect scattering (vacancies and impurity atoms), extended three-dimensional defects (voids), and extended two-dimensional defects (dislocation loops and grain boundaries). It is assumed that antisite defects have a smaller effect on phonon scattering and are ignored, though this requires further study. (For example, Muto and Tanabe [3] describes significant swelling in

* Corresponding author. Tel.: +1 865 574 9942/423 574 9942; fax: +1 865 241 3650/423 576 8424.
E-mail address: sneadll@ornl.gov (L.L. Snead).

0022-3115/$ - see front matter © 2004 Elsevier B.V. All rights reserved.
doi:10.1016/j.jnucmat.2004.11.009

SiC associated with antisite defects. It could be inferred that this mechanism would contribute significant phonon scattering.) It is further assumed that interstitial defects have sufficient mobility at the temperatures considered (>30 °C) to aggregate into dish loops. Additionally, in evaluating Eq. (1), resistive intrinsic three-phonon processes (umklapp) must be considered.

At low temperature, i.e., well below the Debye temperature (θ_D) for a particular material, the temperature dependence of the thermal resistance due to the various scattering mechanisms varies widely, depending on the frequency dependence of the relaxation time. At temperatures above approximately $\theta_D/3$ (~50 °C for alumina, ~125 °C for SiC) however the thermal resistance for all defects is independent of temperature and the thermal resistance due to umklapp scattering is proportional to temperature [1,2].

The room temperature thermal conductivities of some non-irradiated ceramic materials can rival or exceed high conductivity metals such as pure copper (~400 W/m K). Examples include pyrolytic graphite (~1000 W/m K), silicon carbide (~490 W/m K), and beryllium oxide (~240 W/m K). The key to achieving high thermal conductivity in ceramics is to have a highly perfect crystal with low impurities. While there is no way to mitigate the thermal resistance due to umklapp scattering, both the grain boundary and intrinsic defect scattering terms can be significantly reduced by moving towards single, 'perfect' crystals. Indeed, the theoretical conductivity near room temperature for 'perfect' graphite following Taylor's analysis [4] is ~2200 W/m K, significantly above that measured in the best present-day graphitic materials.

The sensitivity of thermal conductivity to point defects makes this property acutely affected by low-temperature neutron irradiation. Since the mobility of point defects and the spontaneous point defect recombination volume in most ceramics are quite low as compared to metals [5,6], fast neutron damage can produce large populations of stable simple defects and defect clusters in ceramics. These defects have been shown to reduce the room temperature thermal conductivity by orders of magnitude for graphite [4,7–19], silicon carbide [20–25] and a range of other ceramics and glasses after neutron irradiation near room temperature to doses $\leqslant$1 dpa.

Various parameters have been used in the literature to categorize the change in thermal conductivity of irradiated ceramics. The most frequently used parameters normalize to the non-irradiated thermal conductivity at some temperature. Examples are the fractional change in conductivity, $(K_{unirr} - K_{irr})/K_{unirr}$, the residual conductivity (K_{irr}/K_{unirr}), and the fractional change in thermal resistance $(W_{irr} - W_{unirr})/W_{unirr}$ where W is the thermal resistivity, $1/K$. The subscripts 'irr' and 'unirr' refer to the conductivity in the irradiated and non-irradiated state, respectively. The fractional change in thermal resistance has been widely used in the graphite literature. Representing the thermal conductivity degradation with these parameters provides a convenient representation of a specific material's thermal conductivity for a particular irradiation environment. However, these parameters are not satisfactory for investigating whether the same underlying physical processes are responsible for the degradation in different grades of a material. In addition, the radiation-induced thermal resistance for different ceramic materials cannot be conveniently compared with this type of analysis.

In the following, a basic theory for the effect of various types of irradiation-induced defects is discussed. Following this discussion, a simple parameter, defined as the added thermal resistance caused by neutron irradiation ($W_{irr} - W_{unirr}$ or $\Delta 1/K$), is used as a tool to understand and compare the thermal conductivity degradation of various ceramics.

1.1. Theory

The integral in Eq. (1) may be evaluated in order to determine the effect of the various scattering mechanisms on the thermal conductivity. At temperatures above $\theta_D/3$, $S(\omega) = 3k_B\omega^2/2\pi^2v^3$ in the Debye approximation, where k_B is Boltzmann's constant.

The phonon relaxation time due to point defects is given by [1,2] $1/\tau_p = A\omega^4$, where A is proportional to the defect density. For vacancies, $A = 9C_v\Omega/4\pi v^3$, where C_v is the vacancy concentration per atom and Ω is the atomic volume. The intrinsic relaxation time is of the form [1,2,26–28], $1/\tau_u = B\omega^2$, where B is a parameter which is proportional to temperature and is given by [1,2]: $B = vT/aT_m\omega_D^2$, where T_m is the melting temperature, a is a parameter on the order of the interatomic distance, T is the temperature, and ω_D is the Debye frequency. Substituting these relaxation times into Eqs. (1) and (2) the increase in thermal resistance due to point defect scattering is found to be [27,28]:

$$\Delta\left(\frac{1}{K}\right) = \frac{1}{K_p} - \frac{1}{K_i} = \frac{1}{K_i}\left(\frac{\omega_D}{\omega_p}\left(\arctan\left(\frac{\omega_D}{\omega_p}\right)\right)^{-1} - 1\right), \quad (3)$$

where K_p is the thermal conductivity with point defect scattering, K_i is the thermal conductivity with intrinsic scattering only, and ω_p is the frequency at which the intrinsic relaxation time is equal to the point defect relaxation time, $\omega_p^2 = B/A$. There are two limiting cases of Eq. (3), for weak vacancy scattering $\omega_p > \omega_D$, and the inverse tangent function may be expanded to obtain,

$$\Delta\left(\frac{1}{K}\right)_{vac} = \frac{1}{3K_i}\left(\frac{\omega_D}{\omega_p}\right)^2 = \frac{3\pi\Omega\omega_D}{2k_Bv^2}C_v. \quad (4)$$

This expression is independent of temperature above $\theta_D/3$ and proportional to the point defect concentration. In the case of strong point defect scattering, $\omega_p < \omega_D$, Eq. (3) becomes

$$\Delta\left(\frac{1}{K}\right)_{vac} = \frac{2}{\pi K_i}\left(\frac{\omega_D}{\omega_p} - \frac{\pi}{2}\right) = \frac{6\pi^{1/2}}{k_B}\frac{1}{\omega_D}\left(\frac{\Omega}{aT_m}\right)^{1/2}(C_v T)^{1/2} - \frac{2\pi^2}{k_B}\frac{v^2}{aT_m\omega_D^3}T. \quad (5)$$

From this expression it is seen that the increase in thermal resistance at a particular temperature will increase as the square root of point defect concentration in this limit.

Planar defects in the form of dislocation loops have a relaxation time of the form [29], $1/\tau_{loop} = C\omega^2$ where in terms of material parameters $C = (24\pi h^2 R^2/v)n_{loop}$, where h is the thickness of the loop, R is the radius of the loop and n_{loop} is the density of loops per unit volume. The increase in thermal resistance is given by

$$\Delta\left(\frac{1}{K}\right)_{loop} = K_i\frac{C}{B} = \frac{24\pi h^2 R^2}{v}n_{loop}. \quad (6)$$

Thus the increase in thermal resistance due to scattering by dislocation loops is proportional to loop density and is independent of the temperature $\theta_D/30$. It is noted that the loops are transparent to phonons of frequency less than approximately $0.2\omega_D$ and so only phonons of frequency greater than this will be scattered by loops. However this is in the region in which point defect scattering becomes important and the processes will compete. For vacancy concentrations greater than approximately 0.001 atomic fraction, point defect scattering will dominate at room temperature and scattering by loops will become unimportant.

The extended defects to be considered here are irradiation-induced voids. The relaxation for these imperfections is given by [27,30], $1/\tau_{ext} = D = N(\pi r^2)v$, where N is the number of defects per unit volume and r is the radius of the defect. Using this relaxation time the increase in thermal resistance due to scattering by voids is [27]:

$$\Delta\left(\frac{1}{K}\right)_{void} = \frac{1}{K_i}\left(\left(1 - \frac{\omega_E}{\omega_D}\arctan\left(\frac{\omega_D}{\omega_E}\right)\right)^{-1} - 1\right), \quad (7)$$

where ω_E is the frequency at which the scattering by voids is equal to the intrinsic scattering, $\omega_E^2 = D/B$. For any expected defect concentration, N, the phonon mean free path due to scattering by voids will be much greater than the interatomic distance and so $\omega_E < \omega_D$. For example, for the case of alumina at 130 °C, ω_E is equal to ω_D when $N\pi r^2 = 4.8\times10^8\ m^{-1}$. For voids with a radius of 10 nm this corresponds to a density of $N = 1\times10^{24}\ m^{-3}$ yielding a volume fraction of 6.4, clearly an impossibility. Using $\omega_E < \omega_D$ Eq. (6) becomes

$$\Delta\left(\frac{1}{K}\right)_{void} = \frac{\pi^3 v}{k_B\omega_D^2}(BD)^{1/2} = \frac{\pi^{7/2}}{k_B}\frac{v^2}{\omega_D^3 T_m^{1/2}a^{1/2}}rN^{1/2}T^{1/2}, \quad (8)$$

which shows that the increase in thermal resistance due to voids is proportional to the square root of both temperature and defect concentration. Section 4 points out that for the irradiation conditions of this study (~60 °C) void formation is not expected in the investigated ceramic materials.

The increase in defect resistance in terms of material parameters, defect size, and defect density is given by Eqs. (5), (6), and (8) for vacancies, dislocation loops, and voids, respectively. Eq. (2) suggests that thermal resistances due to each scattering mechanism may simply be added and that the combined effect will be given by adding these expressions. This however is true only in the case in which three-phonon normal scattering dominates, the so-called Ziman limit. In the case of irradiated materials normal processes will not dominate, and a better approximation for combining separate defect terms is to add the corresponding reductions in thermal conductivity. Thus in general if the effects of the individual scattering mechanisms are to be combined the resulting increase in thermal resistance is given by

$$\Delta\left(\frac{1}{K}\right)_{total} = \frac{1}{K_i}\left\{\left[1 - \left(1 - \frac{\omega_p}{\omega_D}\tan^{-1}\frac{\omega_D}{\omega_p}\right) - \left(\frac{\omega_E}{\omega_D}\tan^{-1}\frac{\omega_D}{\omega_E}\right) - \left(\frac{C}{B+C}\right)\right]^{-1} - 1\right\}. \quad (9)$$

2. Experimental procedure

Twelve commercial ceramic materials were selected for this irradiation study and are listed in Table 1 along with their room temperature physical properties. Of importance is that for some of the materials (SiC and Al_2O_3) different ceramic grades are used to obtain different non-irradiated thermal conductivities for nominally equivalent base materials. A further description of some of these materials is given elsewhere [31]. All materials were machined into cylinders of 6 mm diameter. The length of the samples varied from 3 mm to 10 mm depending on their non-irradiated thermal conductivities, with the longer lengths corresponding to the higher-conductivity materials. Samples were irradiated in the HT-3 position of the HFIR Hydraulic Tube facility at a fast and thermal neutron flux of 7.8×1018 n/m^2 s ($E > 0.1$ MeV) and 2.2×1019 n/m^2 s, respectively. For all samples, a dose equivalent of 1 displacement per atom (dpa) = 1×10^{25} n/m^2 ($E > 0.1$ MeV) was used,

Table 1
Non-irradiated room temperature properties of the ceramics used in this study

	Density, g/cc (%td)	Specific heat, J/kg K	*K*(vendor), W/m K	*K*(measured), W/m K
Morton CVD SiC	3.203 (99.6)	620	320	246
Carborundum Hexoloy-SA SiC	3.08 (95.7)	620	125.6	105
GE siliconized SiC	2.93 (91.1)	620		91
Coors AD-94 Al_2O_3	3.61 (90.7)	880	18.0	18
Coors AD-998 Al_2O_3	3.89 (97.7)	880	29.4	31
Wesgo AL-998 Al_2O_3	3.90 (98.0)	880	29.3	32
Crystal systems sapphire	3.98 (100)	880	40	42
Cercom single crystal $MgAl_2O_4$	3.58 (99.4)	880	~14	19
Cercom aluminum nitride	3.25 (99.7)	1050	115	111
Cercom hot-pressed silicon nitride	3.3 (95.9)	680	~29	36
Brush-Wellman 995 BeO	2.85 (94.7)	1047	251	239
Mitsubishi-Kasei MFC C/C composite	1.93	718	555	520

which is the calculated relationship for these low-atomic-mass ceramics assuming a sublattice-averaged displacement energy of 40 eV [32,33]. The irradiation doses were equivalent to 0.001 dpa and 0.01 dpa for the 60 °C irradiations, and 0.01 and 0.1 dpa for the 300 °C irradiations. In addition to the point defect accumulation due to fast neutrons, the production of helium from the ^{9}Be(n/α) reaction will produce additional *K*th degradation in BeO due to the recoiling atoms and transmutation products. However, due to the low level of helium generation in this study, 1 and 10 appm for 0.01 and 0.1 dpa in BeO, respectively, this process is ignored.

A low-temperature perforated rabbit capsule was used to irradiate the samples in contact with the coolant water (~60 °C). A second rabbit capsule design was used to irradiate at elevated temperatures where the samples were in contact with a graphite sleeve which was slid inside an aluminum capsule and sealed in a helium cover gas. The outside of the aluminum capsule was in contact with the coolant water and the heat generated by the ~45 W/g nuclear heating was conducted across the ~0.25 mm machined gap between the graphite sleeve and the inside of the aluminum tube, thus achieving a calculated temperature of ~300 °C. A single perforated rabbit capsule containing only chemically vapor deposited (CVD) SiC and Coors AD-94 alumina was also irradiated to ~2.6 dpa.

The room temperature thermal diffusivity of the samples was measured with a custom-built xenon thermal flash apparatus. The pulse length and maximum power output of the xenon flash lamp are 0.8 ms and 4800 W s, respectively. With the exception of the dark gray silicon carbide and C/C samples, all materials were coated with a thin film of graphite on the front and rear surfaces in order to make the samples opaque to the Xe flash lamp. Following the thermal flash on the front surface, the rear surface temperature was measured by the infrared signal using an InSb detector, and the diffusivity was calculated following Clark and Taylor's analysis [34]. Density and thickness values corresponding to the non-irradiated or irradiated condition were used for the non-irradiated and irradiated measurements, respectively. For the thermal diffusivity calculations, the density was calculated from dry weight and physical dimension measurements. Some specimen densities were also obtained with density gradient columns using mixtures of tetrabromoethane–methylene iodide or ethylene bromide–bromoform [35]. The accuracy of the density measurement was better than 0.001 g/cc based on repeated measurements and consistent for duplicate samples. Silicon carbide samples were immersed in hydrofluoric acid for a period greater than 24 h to remove any surface silica prior to measurement. The only materials which exhibited significant (>0.1%) swelling due to irradiation were the 2.6 dpa, 60 °C Coors AD94 alumina and CVD silicon carbide samples. It is noted that for this irradiation, amorphization of the periphery of the CVD SiC sample occurred leading to a 9.62% swelling. Further study of this sample, as well as single crystal SiC which was amorphized by high dose neutron irradiation at 60 °C is given elsewhere [36,37]. Thermal diffusivity data from this 2.6 dpa irradiated sample corresponds to an amorphous shell around an ~2.8 mm crystalline core and is therefore a measurement of a heterogeneous sample.

The thickness of the samples was chosen to minimize the parasitic heat loss to the sample holder in the thermal flash apparatus. As the thermal conductivity generally decreases significantly with irradiation, the sample thickness was chosen as the minimum thickness that yielded acceptable non-irradiated values. For the low thermal conductivity materials such as spinel and alumina, the thickness was 3 mm, while the thickness of the high thermal conductivity BeO, CVD SiC, and carbon fiber composite (CFC) was 10 mm.

The room temperature thermal conductivity (*K*) was calculated using the measured thermal diffusivity (α),

measured density (ρ), and the vendor's or handbook [38,39] specific heat (C_p) as follows:

$$K = \alpha \rho C_p. \quad (10)$$

The thermal diffusivity of every specimen was measured before and after irradiation. The conversion from thermal diffusivity to thermal conductivity used the assumption that the specific heat remained unchanged with irradiation. This common assumption is known to be valid for graphite [7]. Furthermore, it is well established that the specific heat is not changed by a crystalline to amorphous transformation; for example the specific heat of glass and the crystalline forms of SiO_2 (quartz, crystobalite, and tridymite) are identical [39]. Table 1 gives the non-irradiated density and specific heat values used to convert the thermal diffusivity measurements to thermal conductivity. The last two columns of Table 1 give the manufacturers' quoted values for thermal conductivity and the non-irradiated specimen measurements obtained in this study. General agreement was found between the two columns with the exception of the Morton (now Rohm-Haas) CVD SiC material where a 23% discrepancy in conductivity values occurred. This is thought to be a batch to batch variation in the Morton product. Such variation in different lots of Morton CVD SiC has been previously observed by the authors. Somewhat smaller discrepancies were also observed for the Carborundum Hexoloy-SA SiC (~16% low), the Mitsubishi MFC C/C composite (~5%) and Cercom aluminum nitride (~4%). Measurements with the thermal diffusivity apparatus performed on a standard graphite specimen produced results within ~1% of the calibrated standard value.

Post-irradiation isochronal anneals were carried out in air at 100 °C and 200 °C. Annealing above 200 °C was carried out in flowing argon to a maximum temperature of 1050 °C. The annealing period was 1 h at each temperature. A furnace excursion occurred during the 450 °C anneal in which the sample temperature reached 500 °C for 5 min. For sufficiently rapid annealing kinetics, it may be more appropriate to represent this data as annealed at 500 °C. However, given that these kinetics are unknown, the annealing temperature of 450 °C is assumed.

Error bars have been generated based on the variability of the data both within a measurement series and from repeating each measurement series. In general, the thermal diffusivity measurements were found to be reproducible within 4% for most samples. A series of at least 10 flash lamp 'shots' were taken for each sample mounting and the typical standard error within this set of measurements was as high as 5%. For samples which suffered large decreases in thermal conductivity following irradiation, the measurement error (likely due to increased conduction to the sample holder) tended to increase as the thermal pulse transit time increased. These higher loss samples were remounted, measured three or four separate times and the data for each run were compared and used in the error analysis. Individual errors based on the reproducibility of remounted specimens were used for the error analysis of samples with significant variability. Due to the low conductivity of the 2.6 dpa irradiated CVD SiC sample there was much higher heat loss to the sample holder, which decreased the reliability of the data. The reproducibility was ~20% in this sample.

Thermal diffusivity data were not obtained for most of the $MgAl_2O_4$ spinel specimens due to an unexpected (corrosive) reaction with a Macor™ machinable glass specimen located next to the spinel specimen in each of the irradiation capsules. Accurate data could only be obtained for the spinel sample which was irradiated to 0.01 dpa at 60 °C.

3. Experimental results

3.1. Thermal conductivity

Fig. 1 shows the thermal conductivity degradation for sapphire and the polycrystalline alumina specimens. For all specimens and both irradiation temperatures a decrease in thermal conductivity with increasing dose is observed, with the ~300 °C irradiation exhibiting less degradation than the ~60 °C irradiation. The relatively high conductivity sapphire shows a larger absolute degradation in thermal conductivity compared to the polycrystalline samples. The middle curve of this plot is labeled 99.8% alumina refers to both the Coors AD-998 and Wesgo AL-998 polycrystalline material of 99.8% nominal purity which exhibited nearly identical

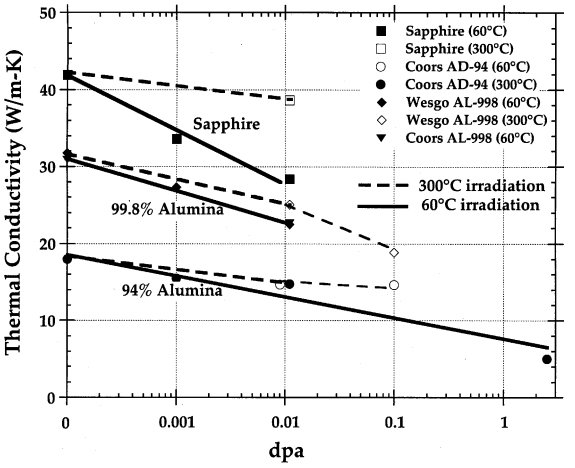

Fig. 1. Thermal conductivity vs. neutron dose for several different grades of Al_2O_3 irradiated at either 60 °C or 300 °C.

behavior. From Table 1 it is seen that both materials are ~98% of theoretical density. The lower curve in Fig. 1 is for the lower nominal purity (94%), lower density (also 94%) Coors AD-94 alumina. The absolute reduction in thermal conductivity for this material was relatively small compared to the higher purity grades of alumina. Due to the small difference in irradiated and non-irradiated diffusivities of AD-94 alumina, the associated error in calculating the defect resistance was relatively large and this was compounded by a higher experimental error due to greater parasitic heat loss in the thermal diffusivity measurement.

Fig. 2 gives the thermal conductivity degradation of the different grades of silicon carbide as a function of fluence. Data trends were similar to that observed for the alumina materials although the magnitude of the changes was larger. In particular, the thermal conductivity degradation was lower at the higher irradiation temperature, and the relative degradation was largest for the highest purity material. The upper curve shows the high conductivity Morton CVD SiC degrading from 245 W/m K to approximately 30 W/m K for the 60 °C, 0.01 dpa irradiation. The general electric siliconized SiC material degraded less in absolute terms but approaches essentially the same as-irradiated value as the CVD SiC at this irradiation condition. The Carborundum Hexoloy™ material gives similar degradation as the siliconized SiC.

The highest fluence data point of Fig. 2 corresponds to the 2.6 dpa irradiation of Morton CVD SiC. Due to the very low conductivity of the irradiated sample, measured as 3.8 W/m K, or ~1.6% of original conductivity, the conduction to the sample holder in the measurement became significant and the curve-fitting routine for the IR temperature measurement produces a large uncertainty. This specimen exhibited a 9.62% volumetric expansion (i.e., decrease in density), and X-ray and TEM diffraction analysis indicated that the material has become amorphous at the periphery (at a radius >~1 mm). A subsequent measurement [40] on fully amorphous SiC has yielded a thermal conductivity of 3.6 W/m K.

The thermal conductivity degradation for silicon nitride and aluminum nitride are shown in Fig. 3. It is seen that the aluminum nitride thermal conductivity has decreased by more than 70 W/m K following the 60 °C, 0.01 dpa irradiation while the silicon nitride has only decreased by about 23 W/m K. In all conditions the silicon nitride has a lower thermal conductivity than that of the aluminum nitride, and in both materials the thermal conductivity values following irradiation to 0.01 dpa at 300 °C were greater than the corresponding 60 °C irradiation values.

Fig. 4 gives the thermal conductivity degradation for beryllium oxide for both the 60 °C and 300 °C irradiations. Again, the specimens irradiated at the higher temperature exhibited less degradation in thermal conductivity. There was no 0.001 dpa, 300 °C irradiated specimen, so the intercept with the non-irradiated conductivity for the 300 °C data set is shown as a dotted line. However, it is expected that the conductivity of BeO specimens irradiated at 300 °C would be higher than the 60 °C data line at any given dose up to 0.1 dpa. The fractional degradation in the thermal conductivity of the BeO specimens was less than that observed in most of the other ceramic specimens. For example, the BeO thermal conductivity following irradiation to 0.01 dpa at 60 °C was ~70% of the non-irradi-

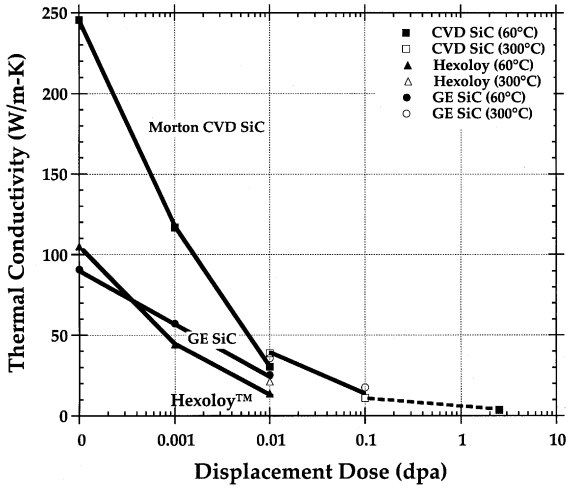

Fig. 2. Thermal conductivity vs. neutron dose for several different grades of SiC irradiated at either 60 °C or 300 °C.

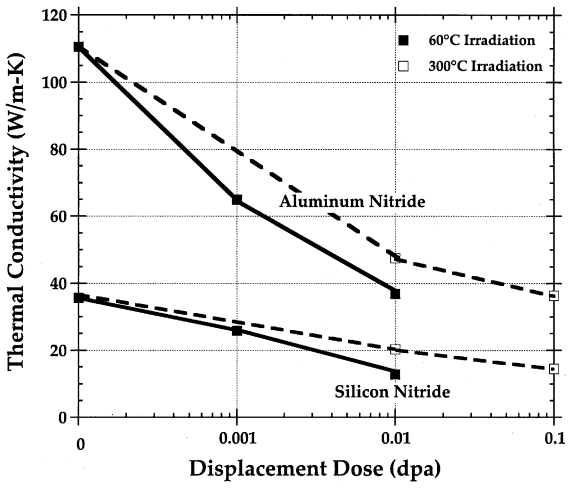

Fig. 3. Thermal conductivity vs. neutron dose for polycrystalline Si_3N_4 and AlN irradiated at either 60 °C or 300 °C.

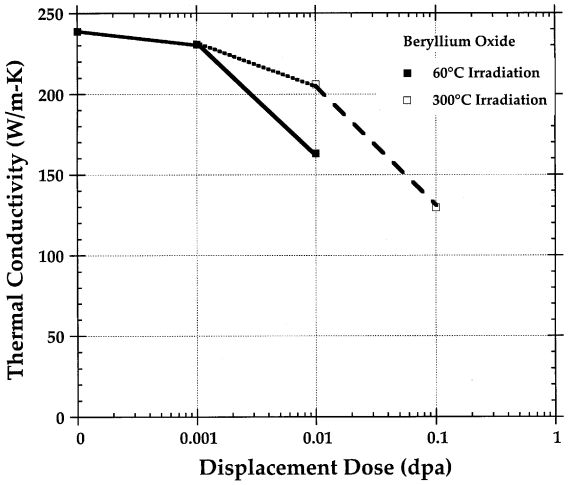

Fig. 4. Thermal conductivity vs. neutron dose for high-conductivity polycrystalline BeO irradiated at either 60 °C or 300 °C.

ated value whereas the corresponding value for CVD SiC (with an non-irradiated conductivity similar to BeO) was only ~12% of the initial thermal conductivity.

Fig. 5 gives the thermal conductivity reduction for the Mitsubishi-Kasei one dimensional carbon fiber composite (MFC-1PH). The data presented in this paper are for the thermal conductivity in the high conductivity direction. The thermal conductivity of this material is extremely anisotropic being ~520 W/m K in the high conductivity (parallel to fiber) direction and ~40 W/m K perpendicular to the fiber direction. The room temperature conductivity decreased to ~10% of the non-irradiated value after irradiation at 60 °C to a dose of only 0.01 dpa. The degradation was less rapid for irradiation at 300 °C, although the conductivity decreased to ~10% of the non-irradiated value after a dose of 1 dpa. A carbon fiber composite specimen was not irradiated in the 0.01 dpa, 300 °C capsule.

3.2. Thermal resistance

In the following plots, error bars for the defect resistance data refer to a combination of the uncertainty within a series of measurements for the non-irradiated and irradiated thermal diffusivities. Error bars refer to ±1-standard error resulting from the difference of two data sets with individual uncertainties (Eq. (5)).

The defect resistances for the sapphire and polycrystalline alumina specimens irradiated at 60 °C to 0.001 and 0.01 dpa are given in Fig. 6. It is clear from Fig. 6 that all of the grades of alumina have similar induced defect resistances at each of the two dose levels studied. A further significant aspect of Fig. 6 is that the defect resistance of all grades of alumina exhibited sublinear dose dependence. Specifically, the defect resistance increased by a factor of ~2.5 as the dose was increased by a factor of 10 (from 0.001 to 0.01 dpa.) Such a sublinear defect accumulation rate has been previously observed for high-purity alumina irradiated with neutrons near room temperature at doses of 10^{-5}–10^{-2} dpa in optical spectroscopy [41,42] and thermal conductivity [43] studies. Assuming the defect resistance is due to point defects or small aggregates of point defects Eq. (4) (weak limit) predicts that the defect resistance would increase linearly if the defect production was linear, and Eq. (5) (strong limit) predicts a factor of $\sqrt{10} \approx 3.2$ increase for a factor

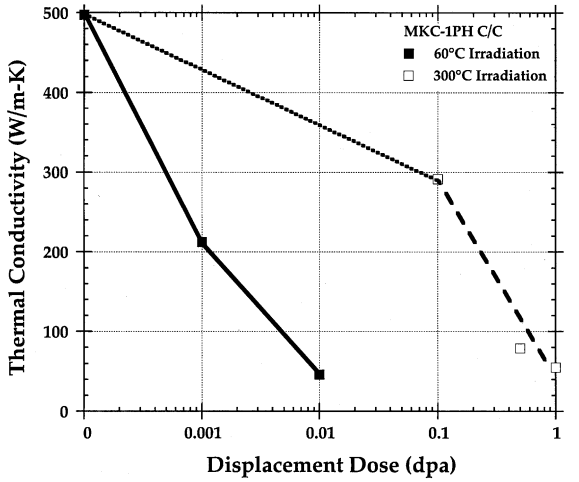

Fig. 5. Thermal conductivity vs. neutron dose for a high-conductivity carbon fiber composite irradiated at either 60 °C or 300 °C.

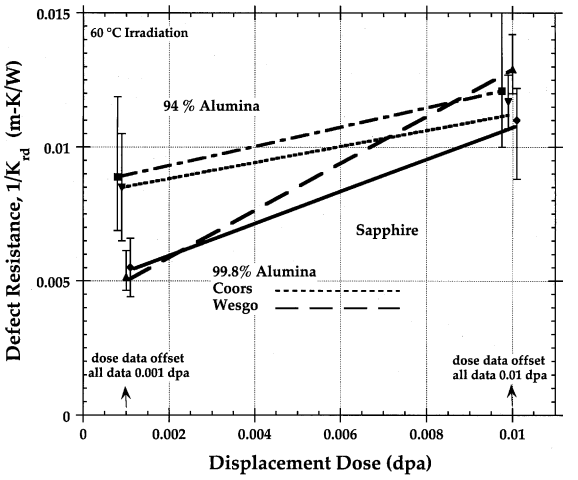

Fig. 6. Radiation-induced defect thermal resistance vs. neutron dose for several different grades of Al_2O_3 irradiated at 60 °C.

of 10 increase in defect concentration. An apparent saturation in the defect resistance has been observed in thermal conductivity measurements of alumina irradiated at 250 °C to damage levels >0.5 dpa [44]. Optical absorption measurements have found a similar saturation in the point defect concentration at doses above ~0.1 to 0.5 dpa for alumina irradiated at room temperature with 3 MeV N^+ ions [45]. The physical significance of the observed sublinear accumulation of defects (Fig. 6) at damage levels far below the room temperature 'saturation dose' of ~0.1 to 0.5 dpa will be discussed in Section 4.

Fig. 7 shows the defect resistance for the three different grades of silicon carbide irradiated at 60 °C. The Morton CVD SiC exhibited the lowest defect resistances and the GE siliconized SiC had a slightly larger defect resistance. The Carborundum Hexoloy™ sintered alpha SiC exhibited about a factor of two higher defect resistance at both irradiation fluences. The physical mechanism responsible for the high defect retention in Hexoloy compared to the other two SiC materials is uncertain. One possibility is that the impurities (or sintering additives) present in Hexoloy SiC somehow enhance the nucleation of defect clusters. Another possible difference between the two powder derived materials (Hexoloy and GE SiC) as compared to the CVD SiC is that the sintering aids such as Si and B will be present in large quantities at the grain boundaries. Irradiation induced differential volumetric expansion which has been shown [22] to dramatically effect strength of hot pressed SiC may play a role in the radiation induced thermal conductivity change due to the grain boundary scattering term which has been assumed constant (see Eq. (1)). All three grades of SiC showed approximately a factor of 5 increase in defect resistance as the dose was increased from 0.001 to 0.01 dpa. This sublinear dose dependence is consistent with the previous work on both thermal conductivity [44,46] and volumetric expansion [44,47] of SiC irradiated with neutrons at ~100 °C. The measured volumetric expansion of the CVD SiC irradiated at 60 °C to 0.001 dpa and 0.01 dpa in the present study was 0.1% and 0.41%, respectively, as measured by the density gradient column technique [35].

3.3. Isochronal annealing of thermal resistance

For the irradiation temperatures and doses of this study, simple defects or defect clusters such as small dislocation loops are the dominant radiation-induced microstructural feature. This has been demonstrated experimentally for SiC [48,49], Al_2O_3 [50,51], graphite [10,52], and aluminum nitride [48,53]. By annealing these ceramics above the temperature at which the irradiation-induced defects were formed, defect recombination (due to dissolution of small vacancy clusters) and an accompanying reduction in the thermal defect resistance occurs. In order to quantify the dose-dependent thermal stability of the defects responsible for the observed radiation-induced increase in thermal resistance, isochronal annealing studies were performed. The effect of isochronal annealing for a period of 1 h on the room temperature thermal resistivity of the ceramics irradiated at 60 °C is shown in Figs. 8–13.

In Fig. 8, the effect of annealing of the defect resistance for polycrystalline alumina and sapphire specimens irradiated to 0.001 and 0.01 dpa at 60 °C is shown. The plot includes the high-purity alumina grades and excludes the lower purity Coors AD-94 because the statistical error of the measurement for AD-94 was com-

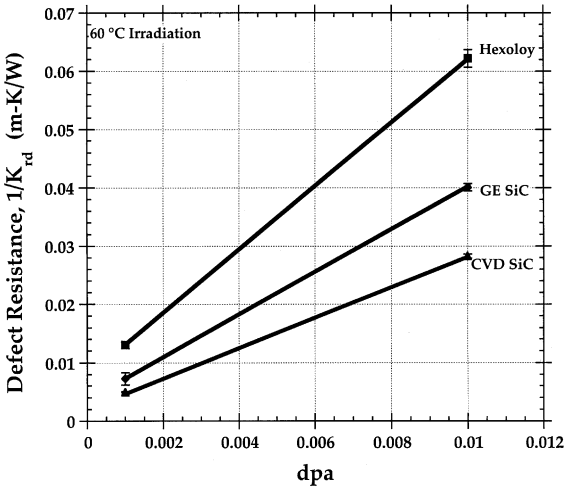

Fig. 7. Radiation-induced defect thermal resistance vs. neutron dose for several different grades of SiC irradiated at 60 °C.

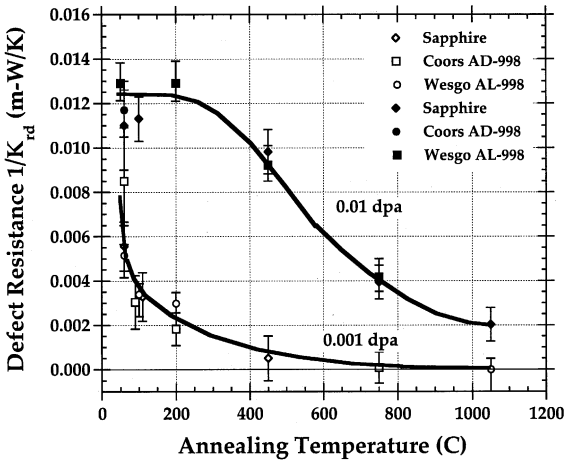

Fig. 8. Annealing behavior of the radiation-induced defect thermal resistance of several different grades of high-purity Al_2O_3 irradiated at 60 °C.

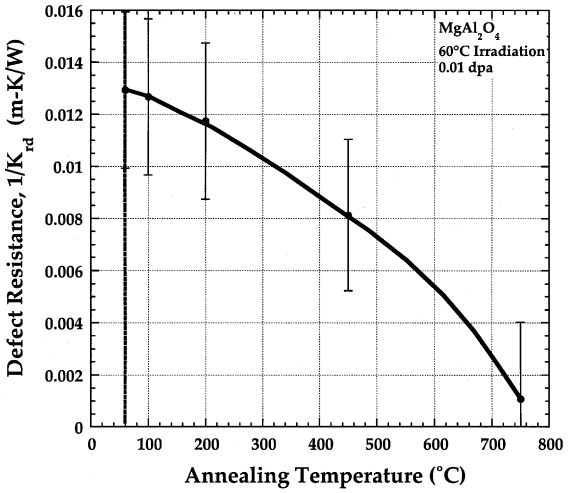

Fig. 9. Annealing behavior of the radiation-induced defect thermal resistance of single crystal $MgAl_2O_4$ irradiated at 60 °C.

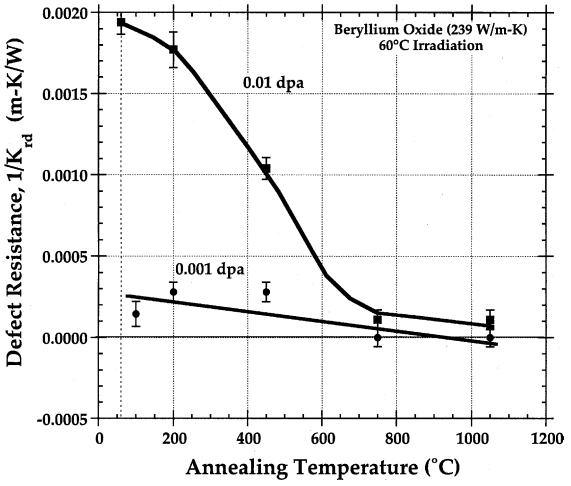

Fig. 10. Annealing behavior of the radiation-induced defect thermal resistance of high-conductivity polycrystal BeO irradiated at 60 °C.

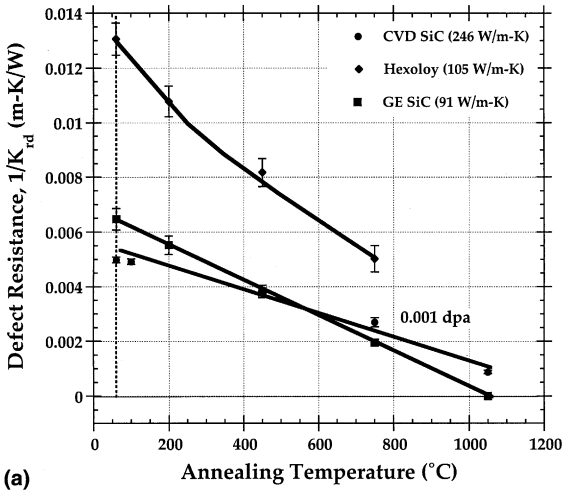

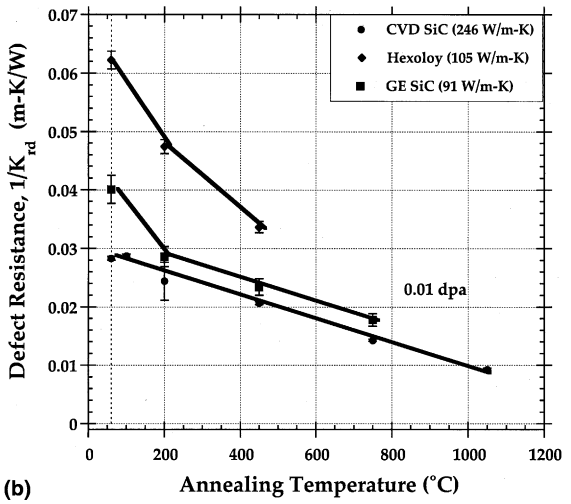

Fig. 11. Annealing behavior of the radiation-induced defect thermal resistance of several different grades of SiC irradiated at 60 °C to a dose of (a) 0.001 dpa and (b) 0.01 dpa.

parable to the observed decrease in defect resistance. Within the scatter in the data there appears to be little difference in the defect-resistance annealing characteristics of the high-purity alumina grades and sapphire. At the lower dose level (0.001 dpa), significant recovery occurs already at 100 °C, after which the recovery is more gradual. Complete recovery of the defect resistance occurs by ~450–750 °C for the 0.001 dpa specimens. For the higher dose irradiation (0.01 dpa), the rate of defect-resistance annealing is somewhat lower than in the 0.001 dpa specimens and some residual defect resistance is still present even at 1050 °C. The higher thermal stability of the defect resistance for the 0.01 dpa specimens suggests that the average defect cluster size has significantly increased between 0.001 and 0.01 dpa. The 0.01 dpa data suggest that a dominant defect annealing stage occurs near 600 °C. Previous optical spectroscopy studies on sapphire irradiated under similar conditions as the present study [42,54–56] have observed several distinct annealing stages in the temperature range from 100 to 800 °C, which are associated with the formation or dissociation of different types of small defects. For example, annealing of oxygen monovacancies occurs in a broad temperature range extending from ~100 °C (i.e., immediately above the irradiation temperature) up to ~700 °C, and oxygen divacancy annealing stages (F_2, F_2^+, etc.) occur at temperatures between 400 and

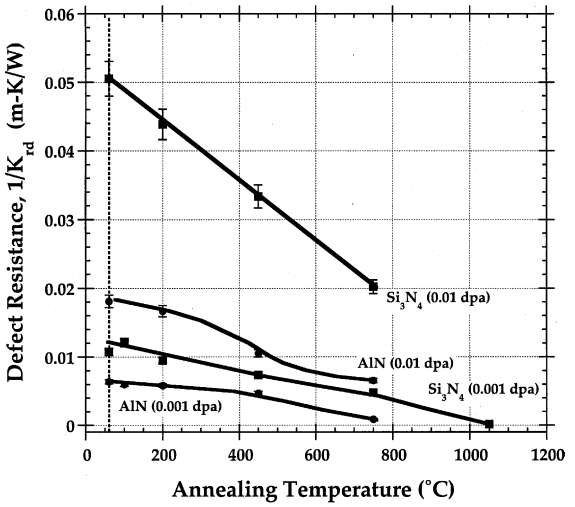

Fig. 12. Annealing behavior of the radiation-induced defect thermal resistance of polycrystalline Si_3N_4 and AlN irradiated at 60 °C.

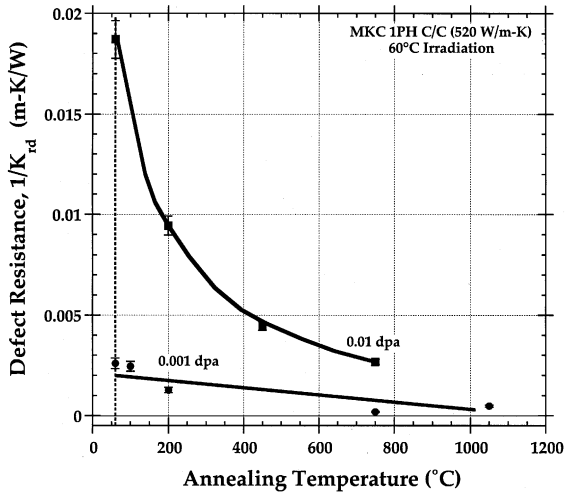

Fig. 13. Annealing behavior of the radiation-induced defect thermal resistance of a high-conductivity carbon fiber composite irradiated at 60 °C.

600 °C. It is expected that the defect resistance of alumina would have similar annealing stages, although the annealing stages may not be as distinct as they are for point defect-specific measurements such as optical spectroscopy since the defect resistance is determined by the combined concentration of point defects and defect clusters. Therefore, annealing of one specific type of defect in a given temperature range has a relatively small impact on the overall defect resistance, unless that defect is predominantly responsible for the thermal conductivity degradation. In addition, the ~100 °C annealing temperature increments used in this study are insufficient to determine if fine structure exists in the annealing curves.

The annealing behavior of spinel irradiated to 0.01 dpa at 60 °C is shown in Fig. 9. Annealing occurred at temperatures slightly above the irradiation temperature, and nearly complete recovery of the defect resistance was observed at 750 °C. The defects in spinel exhibited lower thermal stability than the defects in Al_2O_3 irradiated under the same conditions. As shown in Fig. 8, about 33% of the initial defect resistance was present in the 0.01 dpa Al_2O_3 specimens following annealing at 750 °C, whereas the $MgAl_2O_4$ specimen had <10% of its initial defect resistance following exposure at this annealing temperature.

Fig. 10 shows the annealing behavior of BeO irradiated at 60 °C to 0.001 and 0.01 dpa. Since the defect resistance of BeO irradiated to 0.001 dpa was comparable to the experimental resolution limit, defect annealing was unmeasurable in this specimen. Pronounced defect annealing occurred in the 0.01 dpa specimen at temperatures $\geqslant$200 °C, and nearly complete recovery of the defect resistance occurred at ~750 °C. Annealing of defect resistance has been shown previously to occur in BeO irradiated to low doses at cryogenic temperatures and annealed at temperatures as low as 90 K [57]. BeO irradiated at ~100 °C to doses slightly higher than the present study was reported to show complete recovery of the thermal conductivity degradation by 1200 °C [58].

The defect-resistance annealing of the three grades of silicon carbide irradiated at 60 °C is shown in Fig. 11(a) and (b) for the 0.001 and 0.01 dpa levels, respectively. In all cases, the defect resistance begins to anneal at temperatures slightly above the irradiation temperature. The Morton CVD and GE siliconized SiC samples annealed with an approximately linear slope while the Hexoloy samples had a slightly larger annealing slope up to 200 °C compared to the slope of the recovery curve at higher temperatures. The defect resistance for Hexoloy remained higher than both the Morton CVD SiC and the GE siliconized SiC at all annealing temperatures. Complete recovery of the defect resistance occurred at an annealing temperature of ~1050 °C in the CVD and siliconized SiC specimen irradiated to 0.001 dpa, whereas ~30% of the defect resistance was still present in the 0.01 dpa samples after annealing up to 1050 °C. Previous work has shown that the annealing of the irradiation-induced swelling in SiC is a sensitive measure of the irradiation temperature, and this is one reason for the widespread use of SiC as temperature monitors in irradiation experiments [59–64]. From this nearly continuous recovery behavior, it is inferred that there is a spectrum of defect energies for irradiated SiC in the usual range for temperature monitor applications, 100–900 °C. The annealing trends for SiC irradiated to 0.01 dpa (Fig. 11(b)) appear to be in general agreement with previous work which reported complete

recovery of the defect resistance in Crusilite SiC irradiated to ~0.1 dpa at 250 °C after annealing to 1400 °C [44]. Fig. 11(b) is also in general agreement with the work of Rohde [65] for both HIPped and CVD SiC which were irradiated to ~0.04 dpa at 80 °C. Replotting Rohde's data in similar fashion to Fig. 11 it can be shown that the defect resistance is identical for his HIPped and CVD SiC and that the isochronal annealing data are nearly linear with respect to temperature with the same annealing slope for both materials. The defect resistance in Rohde's data decreased to zero at approximately 1500 °C. Significantly different annealing behavior was obtained by Lee et al. [21] who reported only a small recovery in thermal diffusivity following a 30 min anneal at 1200 °C, yielding only ~25% of the original thermal conductivity. The dose in the study by Lee and coworkers was ~1.5 dpa, which is significantly higher than the specimens in the present study and the work by Thorne and Howard [44] and Rohde [65]. The higher dose irradiation in the study by Lee et al. may have created larger defect aggregates that remained thermally stable up to very high temperatures.

The annealing behavior of aluminum nitride and silicon nitride for both the 0.001 and 0.01 dpa irradiation at 60 °C is given in Fig. 12. The irradiated Si_3N_4 specimens exhibited less rapid thermal annealing kinetics compared to the AlN specimens. Complete recovery of the defect resistance in silicon nitride irradiated to a dose of 0.001 dpa required annealing at ~1050 °C. The annealing of the Si_3N_4 defect resistance appears to be nearly linear with temperature at both doses. To the authors knowledge, there are no previous isochronal annealing studies of the irradiation induced thermal conductivity degradation of silicon nitride. The AlN specimen irradiated to a dose of 0.001 dpa exhibited nearly complete recovery of defect resistance by ~750 °C, whereas about one-third of the original defect resistance was still present in the 0.01 dpa specimen after annealing at 750 °C. This increased thermal stability at 0.01 dpa suggests that the defect size has increased in the AlN specimen as the dose was increased from 0.001 to 0.01 dpa. The AlN specimen irradiated to a dose of 0.01 dpa appears to exhibit an enhanced recovery stage at ~300 °C (Fig. 12), though due additional data with smaller annealing steps are needed to confirm this. A pronounced point defect recovery stage at ~250 °C was previously detected in AlN irradiated with fission neutrons at 90 °C to a dose of ~0.0001 dpa [66]. The irradiation-induced property changes in aluminum nitride have been studied in some detail by Yano and coworkers [48,53,67,68]. By replotting his thermal conductivity data [67] for AlN irradiated at ~100 °C to a dose of approximately 0.02 dpa, it can be shown that his measured defect resistance decreases rapidly above the irradiation temperature and the slope gradually decreases until the defect resistance approaches zero at ~1300 °C. Macroscopic length changes were also measured by Yano showing a corresponding decrease to the non-irradiated value at ~1300 °C.

The annealing behavior of the carbon fiber composite irradiated at 60 °C to 0.001 and 0.01 dpa is shown in Fig. 13. Complete recovery of the defect resistance in the specimen irradiated to 0.001 dpa apparently occurred for temperatures below 750 °C. Pronounced annealing of the defect resistance in the 0.01 dpa specimen occurred for temperatures as low as 200 °C, where ~50% of the original defect resistance was observed. About 16% of the initial defect resistance still remained in the 0.01 dpa specimen following annealing at 750 °C. Based on previous work on identical material irradiated at ~150 °C [69] it is expected that full recovery would not occur for annealing temperatures as high as 1400 °C. As previously shown [18] for carbon fiber composites, as the irradiation dose is increased above 0.01 dpa increasingly higher temperatures are required to produce observable annealing of the thermal defect resistance and the total recovery in the material is decreased. This has been attributed to formation of complex defects between the graphite basal plane that are thermally stable.

4. Discussion

Significant degradation in the thermal conductivity was observed for a dose of only 0.001 dpa at an irradiation temperature of 60 °C in all of the irradiated materials in the present study except for BeO. The relative amount of degradation observed in the present low-dose, low-temperature irradiations was comparable or greater than the degradation reported in many other studies performed at high irradiation temperatures to much higher damage levels. This demonstrates the strong effect of irradiation temperature on the thermal conductivity degradation. As seen from the data of Figs. 1–5, the amount of thermal conductivity degradation for the 300 °C irradiation was less pronounced as compared to the 60 °C irradiation. By increasing the irradiation temperature from 60 to 300 °C for the common dose of 0.01 dpa the thermal defect resistance is reduced by ~30% for alumina, about 50% for spinel and Si_3N_4 and about 60% for CVD SiC. Obviously, a systematic investigation of the fundamental physical mechanisms responsible for thermal conductivity degradation requires examination of the dose, material, and temperature dependence of the defect resistance.

4.1. Summary of dose and material dependence of thermal resistance

As discussed in Section 1, there are three main components to the radiation-induced thermal resistance,

$1/K_{rd}$: point defects, two-dimensional defects (e.g., dislocation loops and uncollapsed planar defect clusters), and three-dimensional defects (cavities, precipitates). The formation of three-dimensional defects generally requires mobile vacancies. Since vacancy migration typically only occurs at temperatures above ~300 °C in the ceramic materials investigated in the present study [5], cavity formation is not expected to have occurred in any of the specimens irradiated at 60 or 300 °C. Point defects are usually modeled as monovacancies in thermal conductivity analyses. It is interesting to note that the relatively small distortion about a vacancy does not cause significant phonon scattering [70]. Although self-interstitial atoms (SIAs) have a significantly higher phonon scattering cross-section than vacancies due to their higher lattice strain [30], the concentration of isolated SIAs in irradiated materials is generally negligible at all temperatures where SIAs are mobile due to the high driving forces for interstitial cluster formation (due to strain energy and defect binding energy considerations) compared to vacancy cluster formation. As reviewed elsewhere [5], interstitials are apparently mobile in most ceramics at room temperature (see also discussion later in this section). Therefore, we have adopted the usual simplification found in most thermal conductivity analyses that all of the radiation-produced point defects scatter as vacancies or vacancy clusters.

If we assume that the increase in thermal resistance in the sapphire sample irradiated at 60 °C (Fig. 6) is due to an increased in point defect concentration alone, then the defect concentration can be estimated from Eq. (3) to be approximately 1500 and 4000 vacancy parts per million (vppm) for the 0.001 and 0.01 dpa irradiations, respectively. This analysis gives an upper limit to the monovacancy concentration, since the radiation-induced increase in thermal resistance associated with other irradiation-induced defects is ignored. The increased thermal stability of the defect resistance with increasing dose observed in the isochronal annealing study (Fig. 8) suggests that concentration of defect clusters has significantly increased between 0.001 and 0.01 dpa. It is interesting to compare this upper-bound limit for monovacancy concentration with optical spectroscopy (F center) studies performed on sapphire at comparable temperatures and doses. Interpolation of the F center data in [42] for sapphire irradiated with fission neutrons at ~90 °C yields an oxygen vacancy concentration of 8.5 ppm and 26 ppm for 0.001 and 0.01 dpa, respectively. The large difference between the defect concentrations estimated from the optical spectroscopy and thermal resistance analyses may be evidence that the majority of the thermal conductivity degradation is due to defect clusters (divacancies, trivacancies, dislocation loops, etc.) for these irradiation conditions. It is also interesting to note that both the optical spectroscopy [38] and thermal resistance (Fig. 6) measurements indicate a factor of 2.5–3 increase in the defect concentration as the dose is increased from 0.001 to 0.01 dpa.

Figs. 14 and 15 give a compilation of the radiation-induced defect resistances for the various ceramics irradiated in this study at 60 °C and 300 °C, respectively. The CVD SiC and Coors AD-998 materials have been selected to represent the pure SiC and alumina behavior, respectively. It is apparent by comparing the magnitude of the defect resistances and the slope of the thermal resistance vs. dpa line that there is a significant difference in the response of the thermal defect resistance among the materials.

One contributing reason for the material dependence of the defect thermal resistances in Figs. 14 and 15 is their different point defect mobilities. Numerous other factors such as crystal structure, atomic bonding characteristics, recombination volume for spontaneous point defect annihilation, and the relative fraction of clustered vs. isolated point defects produced may also affect the relative defect accumulation behavior of a material. However, to first order, the absolute irradiation induced thermal defect resistance and the rate of defect resistance accumulation rate, $\Delta(1/K_{rd})\Delta\Phi$ in a material can be related to the concentration of point defects since they act as the source for all radiation-induced microstructural evolution processes. According to standard rate theory analyses, the steady state point defect concentrations are inversely proportional to the square root of the interstitial diffusivity (D_i) for recombination-dominant conditions [71]. Therefore, defect accumulation rates should decrease with increasing interstitial mobility under recombination-dominant conditions. At high doses, defect cluster formation eventually causes a transition to a sink-dominant condition [71]. However, due to the high typical vacancy migration enthalpies for

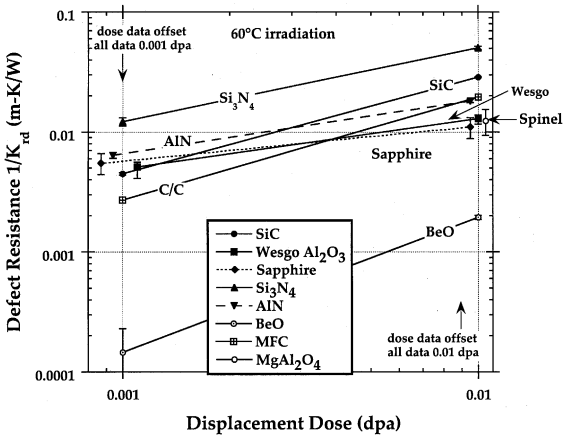

Fig. 14. Comparison of the dose-dependent radiation-induced defect thermal resistances for the ceramics irradiated at 60 °C.

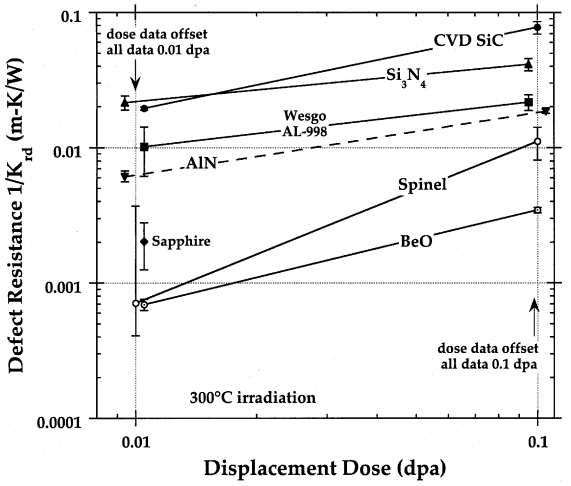

Fig. 15. Comparison of the dose-dependent radiation-induced defect thermal resistances for the ceramics irradiated at 300 °C.

ceramics of ~2 eV [5], the dose required for this transition at 60–300 °C is $P/(D_v C_s) \gg 1$ dpa for typical fission reactor damage rates of $P \sim 10^{-6}$ dpa/s and defect cluster sink strengths of $C_s \sim 10^{15}/m^2$.

Accurate estimates of the interstitial diffusivity are available only for a limited number of ceramics [5]. Recent work has found that the rate-controlling (slower) interstitial migration enthalpy is ~0.21 eV for $MgAl_2O_4$, ~0.6 eV for Al_2O_3 [72]. A recent molecular dynamics simulation by Gao et al. [73] reports interstitial migration enthalpies for SiC as 0.74 eV for carbon and 1.5 for silicon. A relative ranking of ceramics with regard to interstitial mobility can be obtained from the minimum temperature where interstitial mobility has been observed. Table 2 lists the measured critical temperatures for interstitial mobility found experimentally by optical spectroscopy or other methods [Snead, 1997 #609; Atobe, 1987 #18; McDonald, 1963 #470; Atobe, 1990 #534; Zinkle, 2003 #413; Kingery, 1967 #5; Abe, 1997 #402; Wang, 1997 #622; Inui, 1989 #393]. Also given in Table 2 are the melting (or sublimation) temperature and the crystal structure of the materials used in this study. The critical temperature for interstitial migration was estimated from either the minimum temperature where sublinear defect accumulation occurred (at defect concentrations well below saturation) or the critical temperature for ion beam-induced amorphization. Electron irradiation studies were not included in the estimation of the critical interstitial migration temperature, due to possibly large effects of ionization-induced diffusion [41]. To the authors knowledge there are no data from which the critical temperature for interstitial migration in silicon nitride can be accurately determined, though it can be inferred to be <80 K based on the resistance of Si_3N_4 to ion beam-induced amorphization at 80 K up to a dose level of 30 dpa [74].

By simply comparing the critical temperature for the onset of observable interstitial mobility in Table 2 with the defect resistance of the various materials irradiated to 60 °C, 0.01 dpa in Fig. 14, there is a trend for materials with lower critical temperature (i.e., higher interstitial mobility) to have lower defect resistance and lower accumulation slopes $\Delta(1/K_{rd})\Delta\Phi$ One exception to this trend is the defect resistance of the C/C composite, which has a very low (~20 K) interstitial migration energy while having an intermediate defect resistance. However, the crystal structure of graphite is unique. Although it possesses a hexagonal structure as does alumina, aluminum nitride, and beryllium oxide, the distance between the basal planes is quite large and the bonding between these planes is van der Waals rather than ionic. For this reason, the interstitials which are knocked into positions between basal planes are quite mobile and tend to form new planes, but do not easily recombine with vacancies in adjacent basal planes.

As is evident from Eq. (6), the thermal resistance for point defects is proportional to their concentration. From Figs. 6, 7, and 14, it is seen that the defect resistance increased by a factor of two to five as the dose was increased from 0.001 to 0.01 dpa at 60 °C for all of the ceramics investigated. The critical temperature for interstitial mobility in Table 2 can be used to explain the sublinearity of the defect resistance with fluence. In

Table 2
Critical temperature for onset of observable interstitial mobility

Material	T_{crit} (°C)	Ref.	Melting point (°C)	Crystal structure
Al_2O_3	~−70	[5,42,75,76]	2020	Hexagonal
AlN	$-250 < T < 90$	[66]	>2200	Hexagonal
BeO	<−250	[57]	2530	Hexagonal
Graphite	~−250	[77]	3652 sub	Hexagonal
$MgAl_2O_4$	<−170	[5,78]	2128	Cubic
SiC	~30	[36,41]	2698 sub	Cubic
Si_3N_4	<50	[74,79]	>1900	Orthorhomb.

previous work it has been shown for the case of alumina [42], aluminum nitride [66], and beryllium oxide [57] at irradiation temperatures less than the temperature at which interstitials are mobile, that the thermal defect resistance and other properties such as optical absorption are directly proportional to the fluence. However, for temperatures above the critical temperature for interstitial mobility, the defect accumulation rate is sublinear [5,58,66]. This sublinear defect accumulation rate is an indication of uncorrelated defect recombination processes due to long range point defect migration processes [5]. At high damage levels (0.1 dpa or higher) where the defect concentration can become comparable to the saturation defect concentration, sublinear defect accumulation behavior can also be obtained due to the finite probability of spontaneous point defect recombination as displacement cascades begin to impinge on pre-existing radiation defects. However, the defect resistance measured in the present study on alumina and SiC specimens irradiated at 60 °C to 2.6 dpa demonstrate that the saturation defect resistance for these materials is about an order of magnitude higher than the defect resistance measured at 0.01 dpa. Therefore, it is not plausible to attribute the sublinear defect resistance accumulation at 0.001–0.01 dpa to an approach to saturation of the defect concentration.

4.2. Summary of thermal conductivity degradation, defect resistance, and annealing of defect resistance

The conventional practice of plotting the normalized thermal conductivity degradation as a function of irradiation dose is somewhat misleading since grades of a material with higher non-irradiated thermal conductivity show a greater amount of degradation than low-conductivity grades (cf. Fig. 2). However, by comparing the defect resistance accumulation of different grades of the same material (e.g., Figs. 6 and 7), it is seen that the effect of irradiation on the amount of added thermal resistance is generally very similar even for materials with quite different intrinsic thermal conductivities. One advantage of measuring the defect resistance is that the irradiated thermal conductivity of a different grade of the same material with a significantly different non-irradiated conductivity can be estimated from Eq. (3) for a given irradiation condition. The defect resistance measured as a function of irradiation dose and temperature can be applied to other grades of the same material with the provision that they are nominally 'pure' materials. In other words, the defect resistance can be universally applied within a material type as long as the irradiation defect microstructures are similar. The utility of this approach is immediately apparent by inspection of the similarity of the thermal defect resistances for the vastly different grades of alumina in Fig. 6. In contrast, the defect resistance for Hexoloy™ SiC shows a factor of two higher defect resistance as compared to the CVD SiC and GE SiC (Fig. 7). This observation implies that a different type of defect microstructure is present in the Hexoloy™ grade of SiC compared to the other SiC grades, and perhaps associated with the boron sintering aid present in Hexoloy™. Microstructural examination of the different grades of SiC is needed (along with additional higher dose irradiations) in order to better understand the source of this differing behavior.

Another example of the advantage of analyzing defect resistance rather than thermal conductivity is apparent from the silicon nitride and aluminum nitride data. As shown in Fig. 3, the thermal conductivity of AlN decreased by about 70 W/m K while Si_3N_4 decreased by ~20 W/m K following irradiation at 60 °C to 0.01 dpa. The thermal conductivity data plotted in Fig. 3 convey the impression that neutron irradiation is producing more damage in AlN compared to Si_3N_4. However, silicon nitride actually exhibited a larger defect resistance than AlN for these irradiation conditions (cf. Fig. 14). The defect resistance analysis implies that the development of improved grades of Si_3N_4 with higher non-irradiated conductivities would not be a major advantage for neutron irradiation applications in this temperature range, since the conductivity would quickly degrade during irradiation. From Figs. 14 and 15, the most promising materials in terms of fission neutron 'radiation resistance' in the temperature range of 60–300 °C and doses up to 0.1 dpa are BeO, Al_2O_3, $MgAl_2O_4$, and AlN.

5. Conclusions

(1) From an analysis of the data obtained on different grades of the same ceramic material (Al_2O_3), it appears that the thermal defect resistance increase due to neutron irradiation is generally independent of the non-irradiated thermal conductivity even when the non-irradiated conductivities vary by as much as a factor of two or more. Further analysis is needed to determine why the Hexoloy grade of SiC exhibited a significantly different defect resistance behavior compared to other grades of SiC.

(2) For the 0.01 dpa, 60 °C irradiation, the material's susceptibility to radiation-induced increase in thermal defect resistance can be ranked as follows: (1) beryllium oxide, (2) alumina and spinel, (3) aluminum nitride and carbon fiber composite, (4) silicon carbide, and (5) silicon nitride, where beryllium oxide is the least affected by irradiation and silicon nitride exhibits the largest added thermal defect resistance. As the irradiation temperatures increased this relative ranking changed, which has been attributed to different defect kinetics in the various ceramics studied.

(3) The defect resistance of all specimens irradiated at ~60 °C exhibited sublinear dose dependence between 0.001 and 0.01 dpa, and isochronal annealing of the defect resistance occurred at temperatures slightly above the irradiation temperature. Theoretical analysis for the added thermal defect resistance clearly shows that $1/K_{rd}$ is directly proportional to defect density. Both of these observations indicate that at least some point defects (presumably interstitial type) are mobile in all of these ceramics at the irradiation temperature of 60 °C.

(4) The susceptibility of the ceramics to thermal conductivity degradation during neutron irradiation at 60 °C can be roughly correlated with the available data on observed critical interstitial mobility temperature, where materials with higher interstitial mobility have lower radiation-induced thermal defect resistance and a lower defect resistance accumulation rate $\Delta(1/K_{rd})/\Delta\Phi$. Further investigations of the defect resistance increase over a wider range of dose and temperatures, including temperatures below room temperature, are needed to further explore the effect of interstitial mobility on irradiation induced degradation in thermal conductivity.

References

[1] P.G. Klemens, in: F. Seitz, D. Turnbull (Eds.), Solid State Physics, vol. 7, Academic Press, New York, 1958, p. 1.
[2] P.G. Klemens, in: R.P. Tye (Ed.), Thermal Conductivity, vol. 1, Academic Press, New York, 1969, p. 1.
[3] S. Muto, T. Tanabe, J. Appl. Phys. 93 (2003) 3765.
[4] R. Taylor, Philos. Mag. 13 (1966) 157.
[5] S.J. Zinkle, C. Kinoshita, J. Nucl. Mater. 251 (1997) 200.
[6] H. Trinkaus, Mat. Sci. Forum 248&249 (1997) 3.
[7] J.W.H. Simmons, Radiation Damage in Graphite, vol. 102, Pergamon, 1965.
[8] R.J. Price, General Atomics, San Diego, CA, Report GA-A13157, 1974.
[9] R. Taylor, K.E. Gilchrist, L.J. Poston, Carbon 6 (1968) 537.
[10] R. Taylor, K.E. Gilchrist, L.J. Poston, J. Phys. Chem. Solids 30 (1969) 2251.
[11] B.T. Kelly, Carbon 9 (1971) 783.
[12] L. Binkele, High-Temp. High-Press. 4 (1972) 401.
[13] B.A. Thiele, L. Binkele, K. Koizlik, H. Nickel, in: Proc. 16th Int. Symp. on Effects of Radiation on Materials, ASTM, 1992.
[14] T. Maruyama, M. Harayama, J. Nucl. Mater. 195 (1992) 44.
[15] C.H. Wu, J.P. Bonal, B. Thiele, J. Nucl. Mater. 212–215 (1994) 1168.
[16] T.D. Burchell, W.P. Eatherly, J. Nucl. Mater. 179–181 (1991) 205.
[17] T.D. Burchell, W.P. Eatherly, J.P. Strizak, in: A.S. Kumar, D.S. Gelles, R.K. Nanstad (Eds.), Effects of Radiation on Materials: 16th International Symposium, ASTM STP 1175, ASTM, Philadelphia, 1994.
[18] L.L. Snead, T.D. Burchell, J. Nucl. Mater. 224 (1995) 222.
[19] M. Eto et al., J. Nucl. Mater. 212–215 (1994) 1223.
[20] W. Dienst et al., J. Nucl. Mater. 174 (1990) 102.
[21] C.W. Lee, F.J. Pineau, J.C. Corelli, J. Nucl. Mater. 108&109 (1982) 678.
[22] J.C. Corelli, J. Hoole, J. Lazzaro, C.W. Lee, J. Am. Ceram. Soc. 66 (1983) 529.
[23] R.J. Price, J. Nucl. Mater. 46 (1973) 268.
[24] D.J. Senor et al., Fus. Technol. 30 (1996) 943.
[25] L.L. Snead, J. Nucl. Mater., submitted for publication.
[26] P.G. Klemens, G.F. Hurley, F.W. Clinard Jr., in: G.L. Kulcinski, N.M. Burleigh (Eds.), Proc. 2nd Topical Meeting on the Technology of Controlled Nuclear Fusion, CONF-760935, National Tech. Inform. Service, Springfield, VA, 1976, p. 957.
[27] D.P. White, J. Appl. Phys. 73 (1993) 2254.
[28] D.P. White, J. Nucl. Mater. 219 (1995) 165.
[29] D.P. White, Fus. Mater. Semi Annual Report DOE/ER-0313/25, 1999, p. 212.
[30] P.G. Klemens, D.F. Pedraza, Carbon 32 (1994) 735.
[31] R.E. Stoller, Department of Energy Fusion Reactor Semiannual Period Ending 31 March 1990, DOE/ER-031/8, 1990, p. 299.
[32] F.W. Clinard Jr., G.F. Hurley, L.W. Hobbs, J. Nucl. Mater. 108&109 (1982) 655.
[33] L.R. Greenwood, Report DOE/ER-0313/4, 1988.
[34] L.M. Clark, R.E. Taylor, J. Appl. Phys. 46 (1975) 114.
[35] ASTM, D1505-85, Standard Test Method for Density of Plastics by Density Gradient Technique, 1985.
[36] L.L. Snead, S.J. Zinkle, J.C. Hay, M.C. Osborne, Nucl. Instrum. and Meth. B 141 (1997) 123.
[37] L.L. Snead, S.J. Zinkle, Nucl. Instrum. and Meth. B 191 (2002) 497.
[38] S.J. Schneider Jr., in: Ceramics and Glasses, Engineered Materials Handbook, vol. 4, ASM International, Materials Park, Ohio, 1991.
[39] Y.S. Touloukian, E.H. Buyco, in: Specific Heat, Nonmetallic Solids, Thermophysica routes of Matter, vol. 5, Plenum, New York, 1970.
[40] J.C. Bourgoin, Radiat. Eff. Def. Solids 111&112 (1989) 29.
[41] S.J. Zinkle, in: I.M. Robertson et al. (Eds.), Microstructure Evolution During Irradiation, MRS Symposium Proceedings, vol. 439, Materials Research Society, Pittsburgh, 1997, p. 667.
[42] K. Atobe, M. Nakagawa, Cryst. Latt. Def. Amorph. Mater. 17 (1987) 229.
[43] R. Berman, E.L. Foster, H.M. Rosenberg, in: Report of the Bristol Conf. on Defects in Crystalline Solids, Physical Society, London, 1955, p. 321.
[44] R.P. Thorne, V.C. Howard, Proc. Br. Ceram. Soc. 7 (1967) 439.
[45] G.P. Pells, M.J. Murphy, J. Nucl. Mater. 191–194 (1992) 621.
[46] R.J. Price, J. Nucl. Mater. 33 (1969) 17.
[47] R. Blackstone, E.H. Voice, J. Nucl. Mater. 39 (1971) 319.
[48] T. Yano, T. Iseki, Philos. Mag. A 62 (1990) 421.
[49] R.J. Price, J. Nucl. Mater. 48 (1973) 47.

[50] S.J. Zinkle, J.D. Hunn, R.E. Stoller, in: I.M. Robertson et al. (Eds.), Microstructure of Irradiated Materials, MRS Symposium Proceedings, vol. 373, Materials Research Society, Pittsburgh, 1995, p. 299.
[51] H. Abe, C. Kinoshita, K. Nakai, J. Nucl. Mater. 179–181 (1991) 917.
[52] B.T. Kelly, Philos. Mag. 15 (1967) 1005.
[53] T. Yano, T. Iseki, J. Nucl. Mater. 203 (1993) 249.
[54] J.M. Bunch, F.W. Clinard Jr., J. Am. Ceram. Soc. 57 (1974) 279.
[55] K. Atobe, N. Nishimoto, M. Nakagawa, Phys. Status Solidi. (A) 89 (1985) 155.
[56] G.P. Pells, J. Am. Ceram. Soc. 77 (1994) 368.
[57] D.L. McDonald, Appl. Phys. Lett. 2 (1963) 175.
[58] J. Elston, R. Caillat, in: Second United Nations Conference on Peaceful Uses of Atomic Energy, Geneva, Switzerland, 1958, p. 345.
[59] R.J. Price, Nucl. Technol. 16 (1972) 536.
[60] J.E. Palentine, J. Nucl. Mater. 92 (1980) 43.
[61] J.I. Brammgan, A.S. Frazer, W.H. Martin, J. Nucl. Energy 25 (1971) 223.
[62] H. Suzuki, T. Iseki, M. Ito, J. Nucl. Mater. 48 (1973) 247.
[63] H. Miyazaki, T. Suzuki, T. Yano, T. Iseki, J. Nucl. Sci. Technol. 29 (1992) 656.
[64] J.E. Palentine, J. Nucl. Mater. 61 (1976) 243.
[65] M. Rohde, J. Nucl. Mater. 182 (1991) 87.
[66] K. Atobe et al., Jpn. J. Appl. Phys. 29 (1990) 150.
[67] T. Yano, H. Miyazaki, T. Iseki, J. Nucl. Mater. 230 (1996) 387.
[68] T. Yano, T. Iseki, J. Nucl. Mater. 179–181 (1991) 387.
[69] L.L. Snead, T.D. Burchell, 22nd, American Carbon Society, San Diego, CA, 1995, p. 774.
[70] C.A. Ratsifaritana, P.G. Klemens, Int. J. Thermophys. 8 (1987) 737.
[71] L.K. Mansur, J. Nucl. Mater. 206 (1993) 306.
[72] S.J. Zinkle, L.L. Snead, Philos. Mag., submitted for publication.
[73] F. Gao, W.J. Weber, M. Posselt, V. Belko, Phys. Rev. B 69 (2004) 24505.
[74] S.J. Zinkle, L.L. Snead, Nucl. Instrum. and Meth. B 116 (1996) 92.
[75] W.D. Kingery, J. Nucl. Mater. 24 (1967) 21.
[76] H. Abe, S. Yamamoto, H. Naramoto, Nucl. Instrum. and Meth. B 127&128 (1997) 170.
[77] J.W. Corbett, Electron Radiation Damage in Semiconductors and Metals, Academic Press, New York, 1966.
[78] L.M. Wang, S.X. Wang, W.L. Gong, R.C. Ewing, in: I.M. Robertson et al. (Eds.), MRS Symposium on Microstructure Evolution During Irradiation, 439, MRS, 1997, p. 583.
[79] H. Inui, H. Mori, H. Fujita, Acta Metall. 37 (1989) 1337.